MOLECULAR AND CELLULAR BIOLOGY, Sept. 2011, p. 3710–3722 Vol. 31, No. 18
0270-7306/11/$12.00 doi:10.1128/MCB.05140-11

Stanniocalcin 2 Is a Negative Modulator of Store-Operated Calcium Entry▽†

William Zeiger,[1] Daisuke Ito,[2] Carol Swetlik,[3] Masatsugu Oh-hora,[4] Mitchel L. Villereal,[5] and Gopal Thinakaran[3]*

Committee on Molecular Pathogenesis and Molecular Medicine,[1] Department of Neurobiology, Pharmacology, and Physiology,[5] and Departments of Neurobiology, Neurology, and Pathology,[3] The University of Chicago, Chicago, Illinois 60637; Department of Neurology, School of Medicine, Keio University, Tokyo 160-8582, Japan[2]; and Global Center of Excellence Program International Research Center for Molecular Science in Tooth and Bone Diseases, Tokyo Medical and Dental University, Tokyo 113-8549, Japan[4]

Received 31 January 2011/Returned for modification 9 March 2011/Accepted 30 June 2011

The regulation of cellular Ca^{2+} homeostasis is essential for innumerable physiological and pathological processes. Stanniocalcin 1, a secreted glycoprotein hormone originally described in fish, is a well-established endocrine regulator of gill Ca^{2+} uptake during hypercalcemia. While there are two mammalian Stanniocalcin homologs (STC1 and STC2), their precise molecular functions remain unknown. Notably, STC2 is a prosurvival component of the unfolded protein response. Here, we demonstrate a cell-intrinsic role for STC2 in the regulation of store-operated Ca^{2+} entry (SOCE). Fibroblasts cultured from *Stc2* knockout mice accumulate higher levels of cytosolic Ca^{2+} following endoplasmic reticulum (ER) Ca^{2+} store depletion, specifically due to an increase in extracellular Ca^{2+} influx through store-operated Ca^{2+} channels (SOC). The knockdown of STC2 expression in a hippocampal cell line also potentiates SOCE, and the overexpression of STC2 attenuates SOCE. Moreover, STC2 interacts with the ER Ca^{2+} sensor STIM1, which activates SOCs following ER store depletion. These results define a novel molecular function for STC2 as a negative modulator of SOCE and provide the first direct evidence for the regulation of Ca^{2+} homeostasis by mammalian STC2. Furthermore, our findings implicate the modulation of SOCE through STC2 expression as one of the prosurvival measures of the unfolded protein response.

Ca^{2+} ions act as messengers that can alter protein conformation and/or localization, enzymatic activity, and membrane potential, thus initiating signaling networks that underlie cellular processes as diverse as transcription, metabolism, protein folding, cellular communication, motility and adhesion, cellular proliferation, and cell death (11). Accordingly, Ca^{2+} mobility is tightly regulated, and the disruption of Ca^{2+} homeostasis has been shown to be involved in innumerable injury and disease states (7). The endoplasmic reticulum (ER) plays a prominent role in the regulation of cellular Ca^{2+} homeostasis, and proper functioning also requires the maintenance of its own Ca^{2+} stores as the loss of ER Ca^{2+} impairs ER function (41). In nonexcitable cells, Ca^{2+} influx and ER stores serve as the principle sources of Ca^{2+} for cellular signaling (1). Both sources are tightly regulated and coordinated with one another, as Ca^{2+} release from the ER triggers the activation of plasma membrane Ca^{2+} channels in a process known as store-operated Ca^{2+} entry (SOCE) (44). STIM1 recently has been identified as a central regulator of SOCE (32, 46). STIM1 senses Ca^{2+} levels within the lumen of the ER through an N-terminal EF-hand domain, and upon store depletion it oligomerizes and then translocates within ER membranes to bind directly to and activate plasma membrane-localized store-operated Ca^{2+} channels (SOCs) (6). These SOCs vary by cell type but are thought to consist of Orai1 alone or combinations of Orai1 and TRP channel family members (10, 31, 43). In humans, the loss of SOCE due to mutations in STIM1 or Orai1 leads to severe immunodeficiency, muscular hypotonia, and ectodermal dysplasia (16).

Based on the well-characterized role of fish STC as a hormone that regulates Ca^{2+} and phosphate homeostasis by inhibiting gill Ca^{2+} uptake (56–58), mammalian Stanniocalcin proteins (STC1 and STC2) have been widely proposed to be regulators of Ca^{2+} homeostasis (17, 33, 40, 62). However, human STC1 is not detectable in serum under basal conditions and radiolabeled recombinant STC1 is rapidly modified and eliminated, arguing that secreted STC likely functions locally in an autocrine or paracrine manner (13). Consistent with this notion, transgenic mice overexpressing human STC2 have normal serum Ca^{2+} and phosphate levels (17). Likewise, *Stc1*$^{-/-}$, *Stc2*$^{-/-}$, and *Stc1*$^{-/-}$ *Stc2*$^{-/-}$ mice do not exhibit any changes in serum Ca^{2+} or phosphate levels and do not have any deficits in growth or fertility (8, 9). While STC2 does not appear to play a physiologic role in the endocrine regulation of Ca^{2+} homeostasis, numerous studies have demonstrated a link between STC2 expression and a variety of different cancers, including breast, prostate, renal, colorectal, and ovarian carcinomas (4, 5, 22, 36, 51). Other recent work has suggested that STC2 promotes invasiveness and metastasis in cancer cells (26, 29, 53). However, despite a clear role in human disease, the molecular function and targets of mammalian STC2 remain largely unknown.

In addition to being differentially expressed in cancer tissue, STC2 expression also is induced by oxidative stress and hypoxia, indicating that STC2 plays an important role in the cellular response to stress (23, 30). Furthermore, our laboratory

* Corresponding author. Mailing address: Knapp R212, 924 East 57th St., Chicago, IL 60637. Phone: (773) 834-3752. Fax: (773) 834-3808. E-mail: gopal@uchicago.edu.

† Supplemental material for this article may be found at http://mcb.asm.org/.

▽ Published ahead of print on 11 July 2011.

has identified STC2 as a prosurvival component of the unfolded protein response (UPR) whose expression is upregulated by the transcription factor ATF4 through PERK serine-threonine kinase signaling (23). Based on the reciprocal relationship between ER function and Ca^{2+} homeostasis, we hypothesized that STC2 functions at the interface of these processes. Therefore, we have investigated the role of STC2 in the maintenance of cellular Ca^{2+} homeostasis. Using murine embryonic fibroblasts (MEFs) derived from *Stc2* knockout mice, we demonstrate that the loss of STC2 expression leads to changes in cellular Ca^{2+} handling after ER store depletion. These changes result specifically from an increase in Ca^{2+} influx through SOCs. Furthermore, we show that the overexpression of STC2 can reduce SOCE and that STC2 can bind to STIM1 in a stress-dependent manner. These results define a novel cellular function for STC2 and suggest that the regulation of STIM1-mediated SOCE is important for the cellular response to stress.

MATERIALS AND METHODS

Production of *Stc2*$^{-/-}$ mice. The *Stc2* targeting vector was constructed as follows. A 5.0-kb left targeting arm containing 5′ sequences plus the 5′ untranslated region of exon 1, including the nucleotide located at position −1 upstream of the ATG start codon of exon 1, was PCR amplified from genomic DNA of 129SvEv-derived embryonic stem (ES) cells with two primers, S2SAF1 (5′-CAAAGTCAGGCTCATTTGGA-3′) and S2SA2R3 (5′-GGTTCTGGGTATCACCCTCC-3′); a 3.0-kb right arm downstream of exon 2 was amplified using two primers, S2LAF2 (5′-TGAGCAGATTTCCTGGGTTT-3′) and S2LA2R3 (5′-GCAAAATCCAGGATCCTACAG-3′). Both arms were cloned into pN-Z-TK2 vector (kindly provided by R. Palmiter, University of Washington, Seattle, WA). The targeting construct was linearized at the unique AscI site and electroporated into 129SvEv-derived embryonic stem cells. Three hundred eighty-four ES cell clones were screened by Southern blot analysis using flanking 3′ genomic DNA probe external to the targeting vector. One clone (3-104), carrying a disrupted *Stc2* allele, was injected into C57BL/6 mouse blastocysts to produce chimeric mice. Chimeras subsequently were mated with C57BL/6 mice, and once germ line transmission was achieved, heterozygote *Stc2*$^{+/-}$ mice were cross-bred to generate homozygous *Stc2*$^{-/-}$ mice. Genotyping by PCR was performed using tail DNA as a template and a set of four primers: WtF (5′-GCTGTGGTGTGTTTGAGTGTTTCG-3′), WtR (5′-TGCTTATTAGGTTCTCTGCCCTG-3′), KoF (5′-CTGGCGTAATAGCGAAGAGG-3′), and KoR (5′-CGCTCAGGGTCAAAATTCAG-3′). The primers WtF and WtR amplified a 703-bp fragment from the wild-type allele, and primers KoF and KoR amplified a 424-bp fragment from the knockout allele.

Mice were provided food and water *ad lib*, maintained on a 12-h light/12-h dark cycle, and housed under conditions controlled for temperature and humidity. All mouse procedures used in this study were reviewed and preapproved by meeting the Animal Experimentation Guidelines of the Keio University School of Medicine or the Institutional Animal Care and Use Committee at the University of Chicago as appropriate.

Histology. For histopathological studies, brain and peripheral tissues (cerebrum, cerebellum, heart, liver, lung, spleen, pancreas, kidney, testis, and quadriceps femoris muscle) were removed from 3- and 6-month-old wild-type and *Stc2*$^{-/-}$ mice. After fixation with 3.7% formaldehyde in phosphate-buffered saline (PBS) for 4 days, specimens were embedded in paraffin. Sections (7 μm) were cut with a microtome, stained with hematoxylin and eosin, and examined under a light microscope.

Cell culture. Primary fibroblasts were cultured from 13.5-day-old wild-type (WT) and *Stc2*$^{-/-}$ embryos. To induce ER stress, second-passage cells were treated for 16 h with 2 μg/ml tunicamycin (Tm) or 300 nM thapsigargin (Tg) (Sigma). For further characterization, WT and *Stc2*$^{-/-}$ MEFs were immortalized by transfection with a plasmid encoding the simian virus 40 large T antigen. Transformed MEFs and COS cells were cultured in Dulbecco's modified essential medium (DMEM) supplemented with 10% bovine growth serum (HyClone). Immortalized rat hippocampal H19-7 cells were cultured in the same medium at 33°C; to induce differentiation, cells were switched to N2 medium supplemented with 50 ng/ml basic fibroblast growth factor (bFGF) (Gibco) and incubated at 39°C (61). *Stim1*$^{-/-}$ *Stim2*$^{-/-}$ double knockout (dKO) and control MEFs have been described (39). Recombinant retroviruses produced in Plat-E packaging cells were used for transient infections and to generate stable pools of transduced cells (37).

Cell proliferation and viability assays. The proliferation and survival of transformed WT and *Stc2*$^{-/-}$ MEFs was determined using cell counting kit 8 (Dojindo Molecular Technologies). For cell viability assays, MEFs were plated at a density of 10^4 cells per well in 96-well microplates. The following day, cells were exposed to Tg or hydrogen peroxide (H_2O_2) diluted to the indicated final concentrations in the culture medium in triplicate for the indicated times. A standard curve of absorbance values for known cell densities was generated for each experiment.

Plasmids and antibodies. The cDNA encoding mouse *Stc2* (23) was C-terminally modified by the addition of sequence coding for the amino acids RFLEERP (CT11 epitope tag) and KDEL (ER retention signal) to generate $STC2_{CT11}$ and $STC2_{KDEL}$, respectively. The yellow fluorescent protein (YFP)-STIM1 expression vector was a generous gift of T. Meyer (32). The STIM1-myc expression vector was obtained from Addgene (plasmid 17732) (39). For the generation of stable pools, cDNA or *Stc2* RNA interference (RNAi) sequence (23) was subcloned into pMXs (37) or pSUPER.retro (OligoEngine) retroviral plasmid. Two polyclonal antisera against STIM1 were raised in rabbits against the synthetic peptide CPGRKKFPLKIFKKPLKK and characterized using *Stim1*$^{-/-}$ *Stim2*$^{-/-}$ dKO MEFs. Rabbit polyclonal antisera against STC2, GRP78, and flotillin-2 have been described previously (18, 23, 34). Rabbit antiserum CT11 reacts with the residues RFLEERP. Mouse monoclonal antibodies against α-tubulin and green fluorescent protein (GFP) (Invitrogen), 6-glyceraldehyde-3-phosphate dehydrogenase (GAPDH) (Abcam), protein disulfide isomerase (PDI; StressGen), c/EBP homologous protein (CHOP; Santa Cruz), and rabbit polyclonal antibody against calnexin (StressGen) were purchased.

RT-PCR. Total RNA was isolated from 3-month-old mouse kidneys, and the reverse transcription-PCR (RT-PCR) analysis of *Stc2*, *Stc1*, and β-*actin* expression was performed as described previously (23). Total RNA was isolated from WT and *Stc2*$^{-/-}$ MEFs using the RNeasy kit (Qiagen), and cDNA was synthesized using the SuperScript III first-strand synthesis system (Invitrogen). Quantitative PCR then was conducted using SYBR GreenER SuperMix (Invitrogen) and an iCycler thermal cycler (Bio-Rad).

Protein analysis. Cells were lysed in cold lysis buffer (50 mM Tris-HCl [pH 7.4], 150 mM NaCl, 0.5% NP-40, 0.5% sodium deoxycholate, 0.25% sodium dodecyl sulfate, 5 mM EDTA, and protease inhibitor cocktail [Sigma]) and sonicated. Lysates were fractionated by SDS-PAGE on 4 to 20% Tris-glycine gradient gels (Invitrogen) and transferred to polyvinylidene difluoride membranes (Millipore), which were sequentially incubated with primary antibodies and horseradish peroxidase-conjugated protein A or goat anti-mouse IgG (Jackson ImmunoResearch Laboratories). Signals were visualized by enhanced chemiluminescence detection (PerkinElmer Life Sciences). Alternatively, blots were incubated with infrared (IR) dye-conjugated secondary antibodies and visualized by an Odyssey infrared imaging system (LiCor Biosciences).

For coimmunoprecipitation studies, COS cells transfected with STIM1 and/or $STC2_{CT11}$ were lysed in 1% 3-[(3-cholamidopropyl)dimethylammonio]-2-hydroxy-1-propanesulfonate (CHAPSO) buffer (1% CHAPSO, 50 mM HEPES, 150 mM NaCl, 2 mM EDTA, and 10 mM *n*-ethylmaleimide) on ice. Lysates were clarified by centrifugation at 10,000 rpm for 10 min and precleared for 2 h with protein A agarose. Aliquots of lysates then were incubated at 4°C overnight with primary antibodies (polyclonal STIM1 antibody or polyclonal CT11 antibody [to capture tagged STC2]). Immune complexes were collected using protein A agarose, washed three times in 1% CHAPSO buffer, and analyzed by Western blotting using STIM or CT11 antibodies. For the analysis of endogenous STIM1 interaction with STC2, WT and *Stim1*$^{-/-}$ *Stim2*$^{-/-}$ dKO MEFs stably transduced with $STC2_{CT11}$ retrovirus were grown to confluence and treated for 4 h or overnight with 0.5 μg/ml tunicamycin (Tm) or 50 nM thapsigargin (Tg) before lysis and coimmunoprecipitation with STIM1 antibody.

Immunofluorescence labeling. WT and *Stc2*$^{-/-}$ MEFs grown on poly-L-lysine-coated coverslips were fixed in 4% paraformaldehyde and then permeabilized in 0.2% Triton X-100 for 5 min. After blocking, the cells were stained with antibodies against α-tubulin for 1 h and then with Alexa 488-conjugated secondary antibody and 50 μg/ml tetramethyl rhodamine isocyanate (TRITC)-conjugated phalloidin for 1 h at room temperature. Coverslips then were washed and incubated with Hoechst (1:10,000) before final washing and mounting to slides. MEFs stably overexpressing STC2 were stained with polyclonal STC2 antiserum and monoclonal antibodies against immunoglobulin heavy-chain binding protein (BiP; StressGen) or GM130 (BD Transduction laboratories) and detected using secondary antibody conjugates with Alexa 488 and Alexa 555.

For colocalization analysis, COS-7 cells were double stained with antibodies against CT11 and GFP for 1 h and then secondary antibodies for 1 h. Image

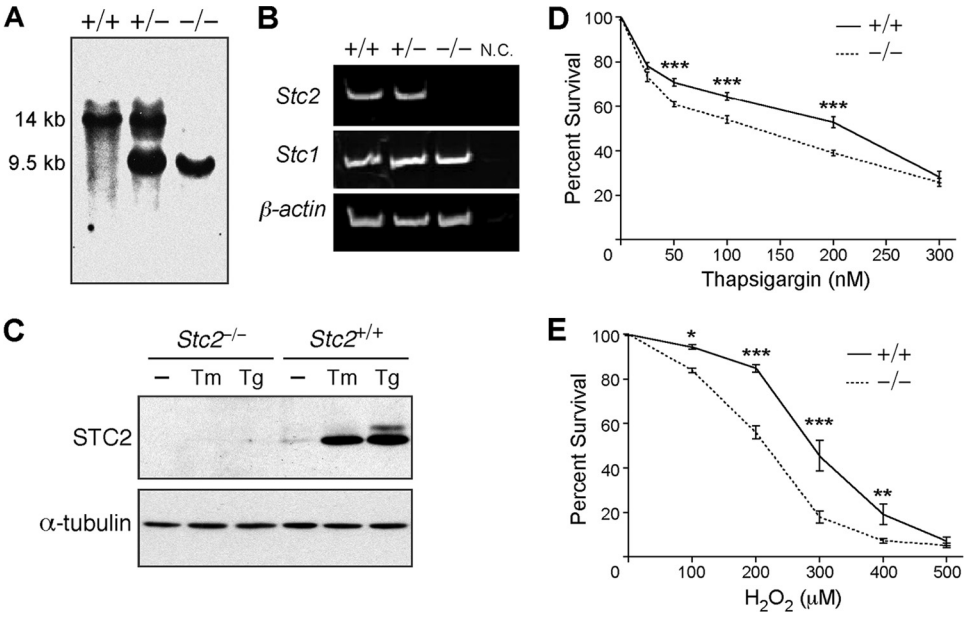

FIG. 1. Characterization of *Stc2*$^{-/-}$ MEFs. (A) Southern blot of mouse tail DNA isolated from *Stc2*$^{+/+}$, *Stc2*$^{+/-}$, and *Stc2*$^{-/-}$ animals. (B) RT-PCR analysis of *Stc2* expression in *Stc2*$^{+/+}$, *Stc2*$^{+/-}$, and *Stc2*$^{-/-}$ kidneys. N.C., negative control RT-PCR without reverse transcriptase. (C) Western blot analysis of STC2 expression in MEFs treated with Tm (2 μg/ml) or Tg (300 nM) for 16 h. WT and *Stc2*$^{-/-}$ MEFs were treated for 8 h with a range of concentrations of Tg (D) or H_2O_2 (E) to elicit ER or oxidative stress. Cell viability was determined using colorimetric WST-8 assays, and percent survival was calculated relative to that of untreated cells. Each point on the graph represents the means ± standard errors of the means (SEM) from at least three independent experiments. *, $P < 0.05$; **, $P < 0.01$; ***, $P < 0.001$ (each by one-way analysis of variance [ANOVA]).

stacks (0.2-μm Z step) were acquired on a Nikon Eclipse TE-2000 E microscope with a 100× (1.45 numeric aperture [NA]) or 60× (1.49 NA) objective and processed using Metamorph software (Universal Imaging Corp.). Z stacks then were deconvolved using Huygens software (Scientific Volume Imaging) and used to quantify Pearson's coefficient of colocalization using the JACoP plug-in for ImageJ (3).

Ca^{2+} imaging. The intracellular Ca^{2+} concentration ($[Ca^{2+}]_i$) was measured in cells loaded with 5 μM Fura-2-acetoxymethyl ester (Fura-2 AM) using a Nikon Diaphot inverted epifluorescence microscope and an InCyt IM2 fluorescence imaging system (Intracellular Imaging Inc., Cincinnati, OH) as previously described (61). Individual responses from ~50 cells per coverslip were monitored and averaged. Each experiment was repeated on at least three independent coverslips.

For experiments using conditioned media, *Stc2*$^{-/-}$ MEFs or stably transduced *Stc2*$^{-/-}$ MEFs overexpressing STC2 (designated KO+STC2) were cultured in flasks in Leibovitz's L-15 CO_2-independent medium overnight. WT or *Stc2*$^{-/-}$ MEFs cultured in coverslips were loaded with Fura-2 AM as described above and then placed in conditioned medium collected from *Stc2*$^{-/-}$ or KO+STC2 MEF flasks and immediately used for imaging. After establishing a baseline in conditioned medium for 5 min, Tg was added directly to the cells in conditioned medium.

For manganese quench experiments, Hanks balanced salt solution (HBSS) was supplemented with 2 mM $MnCl_2$. After establishing the rate of manganese leak in $HBSS^+$ Mn^{2+} medium, cells were challenged with Tg and the decline of Fura-2 fluorescence was monitored over time. Ca^{2+} influx rates then were calculated as the rate of Fura-2 quenching before the addition of Tg (designated Mn leak) subtracted from the rate after Tg challenge (Tg slope).

To assess SOCE in H19-7 cells, barium influx experiments were conducted. Ba^{2+} enters cells through Ca^{2+} channels and binds to Fura-2 but is not sequestered into intracellular stores or pumped by plasma membrane Ca^{2+} ATPases, so changes in the Fura-2 ratio due to Ba^{2+} directly report cation influx rates (27). H19-7 cells were loaded with 5 μM Fura-2 AM, and after establishing the rate of barium leak in Ca^{2+}-free (0 Ca^{2+}) HBSS plus 2 mM $BaCl_2$, cells were challenged with Tg (1 μM) in the absence of extracellular Ca^{2+} and Ba^{2+} to deplete ER stores, followed by the add back of 0 Ca^{2+} HBSS plus Ba^{2+} to trigger SOCE. The Fura-2 fluorescence ratio (F_{340}/F_{380}) was monitored over time, and barium influx was determined as the barium leak rate subtracted from the linear slope of the F_{340}/F_{380} ratio after the add back of 0 Ca^{2+} HBSS plus Ba^{2+} to trigger SOCE.

YFP-STIM1 translocation assay. WT and *Stc2*$^{-/-}$ MEFs stably transduced with YFP-STIM1 were plated on poly-L-lysine-coated 35-mm glass-bottom dishes and placed in HBSS before mounting on the stage of a motorized inverted fluorescence microscope (Nikon Eclipse TE-2000 E with perfect focus) maintained at 37°C using a custom-designed environment chamber. After obtaining a wide-field image of YFP-STIM1 fluorescence, total internal reflection (TIRF) images were acquired every 15 s using a 60× TIRF objective (1.49 NA), YFP filter cube (490- to 510-nm excitation, 520-nm emission; Nikon), and an electron-multiplying charge-coupled device (EMCCD) camera (Photometrics Cascade II). After acquiring baseline TIRF images, cells were briefly washed in 0 Ca^{2+} HBSS and Tg was added to deplete ER Ca^{2+} stores. Images were analyzed using Metamorph imaging software (Molecular Devices). After background subtraction, total YFP fluorescence intensity was measured at each time point for individual cells. Total TIRF YFP signals at baseline (before Tg addition) and at maximum were normalized to the wide-field cellular fluorescence image to calculate the baseline and maximum translocated YFP-STIM1 values. To quantify the kinetics of STIM1 translocation, TIRF YFP signals were normalized to the maximum TIRF YFP signal for each cell and plotted over time. Individual curves then were fit using a Boltzmann nonlinear curve fit in OriginPro (OriginLab Software), and the time to half-maximal translocation (X_0) and rate of translocation (dX) were determined. Puncta size, number, and shape were quantified using the integrated morphometry analysis tool in Metamorph imaging software.

RESULTS

Loss of *Stc2* expression in embryonic fibroblasts confers increased susceptibility to ER and oxidative stress. To investigate the cellular function of STC2, we generated *Stc2* null mice by targeted deletion of exons 1 and 2 (Fig. 1A; also see Fig. S1A in the supplemental material). The loss of *Stc2* expression in *Stc2*$^{-/-}$ animals was confirmed by RT-PCR analysis (Fig. 1B). The expression of *Stc1*, the homolog of *Stc2*, was comparable in all genotypes, indicating a lack of compensatory changes in *STC1* expression in *Stc2*$^{-/-}$ mice (Fig. 1B). The

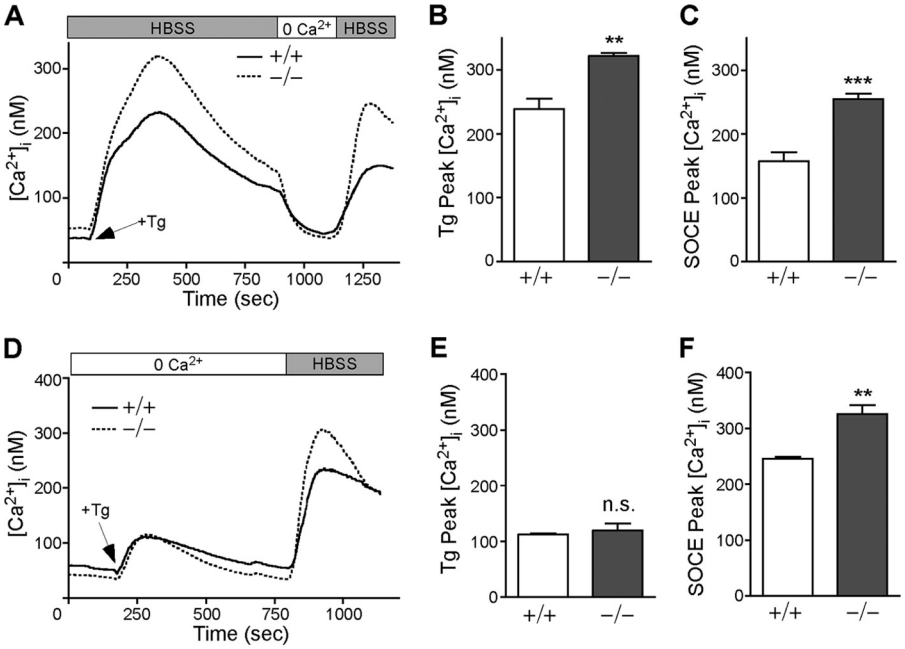

FIG. 2. *Stc2*$^{-/-}$ MEFs display altered Ca^{2+} homeostasis. (A) WT and *Stc2*$^{-/-}$ MEFs loaded with 5 μM Fura-2 AM were treated with Tg (300 nM) in the presence of extracellular Ca^{2+} (1.3 mM Ca^{2+} HBSS), followed by perfusion with 0 Ca^{2+} HBSS and the add back of extracellular Ca^{2+} to trigger SOCE. Traces represent the averages from six to seven experiments each for WT and *Stc2*$^{-/-}$ MEFs. Average peak Ca^{2+} levels (means ± SEM) after the addition of Tg (B) or extracellular Ca^{2+} (C) for SOCE are shown. (D) WT and *Stc2*$^{-/-}$ MEFs were treated with Tg in the absence of extracellular Ca^{2+} before Ca^{2+} add back. Each trace represents averages from five experiments. Graphs represent average peak Ca^{2+} levels (mean ± SEM) after the addition of Tg (E) or extracellular Ca^{2+} (F) for SOCE. **, $P < 0.01$; ***, $P < 0.001$ (each by Student's *t* test).

mating of *Stc2*$^{+/-}$ mice generated pups in the expected Mendelian frequencies, and *Stc2*$^{-/-}$ mice displayed no deficits in viability or fertility or any gross anatomical defects or significant lesions, although they did show a small but significant increase in body weight as previously described (see Fig. S1B to G in the supplemental material) (9).

Primary MEFs cultured from *Stc2*$^{-/-}$ embryos had normal cytoskeletal and morphological structure (see Fig. S2A in the supplemental material), and their proliferation under normal culture conditions was indistinguishable from that of WT MEFs (see Fig. S2B). As expected, STC2 expression was induced in WT but not *Stc2*$^{-/-}$ MEFs following exposure to the ER stress-eliciting agent tunicamycin (Tm) or thapsigargin (Tg) (Fig. 1C). Similarly to our previously published results for astrocytes, N2a, and PC12 cells, increases in STC2 protein expression in WT MEFs were clearly visible after 4 h of treatment and continued to increase even after 16 h (see Fig. S2C). To determine whether *Stc2* expression is required for the optimal induction of the UPR, we exposed WT and *Stc2*$^{-/-}$ MEFs to different concentrations of Tg (ranging from 25 to 300 nM) and monitored the upregulation of well-established markers of the UPR. Immunoblot analysis revealed robust and comparable increases in the levels of BiP, PDI, and CHOP following the addition of Tg in both WT and *Stc2*$^{-/-}$ MEFs (see Fig. S2D). Nevertheless, *Stc2*$^{-/-}$ MEFs demonstrated significantly decreased survival compared to that of WT MEFs after exposure to Tg or H_2O_2 (Fig. 1D and E). Therefore, *Stc2* expression is important for cell survival in response to ER and oxidative stress.

***Stc2*$^{-/-}$ MEFs display altered Ca^{2+} homeostasis.** Although widely implicated in mammalian mineral homeostasis, a direct role for STC2 in Ca^{2+} handling has never been demonstrated. To determine whether STC2 plays a role in intracellular Ca^{2+} homeostasis, we conducted the fluorescent imaging of WT and *Stc2*$^{-/-}$ MEFs loaded with the ratiometric dye Fura-2. After establishing $[Ca^{2+}]_i$ baselines in HBSS (containing 1.3 mM extracellular Ca^{2+}), Tg, an irreversible inhibitor of the sarcoendoplasmic reticulum Ca^{2+} ATPase, was added to deplete ER Ca^{2+} stores (52). Subsequently, extracellular Ca^{2+} was removed by perfusion with 0 Ca^{2+} HBSS before being added back (HBSS containing 1.3 mM extracellular Ca^{2+}) to trigger SOCE (Fig. 2A). Quantitative PCR analysis revealed that *Stc2* expression remained unchanged throughout the time span of this experiment, which is typically between 20 and 30 min (see Fig. S3A and B in the supplemental material). Although WT and *Stc2*$^{-/-}$ MEFs showed no difference in $[Ca^{2+}]_i$ baselines, peak Ca^{2+} levels induced by Tg treatment in the presence of external Ca^{2+} were significantly increased in *Stc2*$^{-/-}$ MEFs compared to those of the WT (Fig. 2B). Since this increase represents both Ca^{2+} loss from the ER store and extracellular Ca^{2+} influx through SOCs, we also quantified $[Ca^{2+}]_i$ peaks following washout with 0 Ca^{2+} HBSS and Ca^{2+} add back to isolate the SOCE component. We found that the SOCE peak also was significantly higher in *Stc2*$^{-/-}$ than in WT cells (Fig. 2C). Quantitative differences in $[Ca^{2+}]_i$ after store depletion were consistently observed in independent pools of WT and *Stc2*$^{-/-}$ MEFs cultured from multiple embryos (see Fig. S3C). In the absence of extracellular Ca^{2+}, the Tg-induced Ca^{2+}

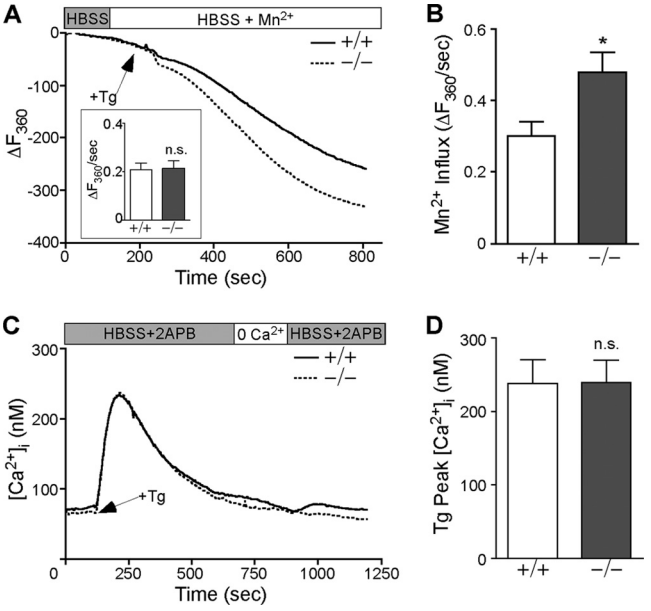

FIG. 3. Store-operated Ca^{2+} entry is increased in *Stc2*$^{-/-}$ MEFs. (A) Fura-2-loaded WT and *Stc2*$^{-/-}$ MEFs were perfused with HBSS containing 2 mM $MnCl_2$, followed by treatment with Tg (300 nM). Images were acquired at an excitation of 360 nm (the isosbestic point for Fura-2). Traces represent averages from at least 15 experiments. The inset shows average Mn^{2+} leak rates before the addition of Tg. (B) Average Mn^{2+} influx rate (corrected for Mn^{2+} leak) after Tg addition (means ± SEM). (C) WT and *Stc2*$^{-/-}$ MEFs loaded with Fura-2 were perfused with HBSS containing 50 μM 2-APB, a specific inhibitor of SOCE, followed by treatment with Tg, perfusion in 0 Ca^{2+} HBSS, and Ca^{2+} add back in the presence of 2-APB. Traces represent averages from nine experiments. (D) Quantification of average $[Ca^{2+}]_i$ peaks after Tg addition (means ± SEM) in the presence of HBSS and 2-APB. *, $P < 0.05$ by Student's *t* test.

peak did not differ between WT and *Stc2*$^{-/-}$ MEFs (Fig. 2D and E), indicating that the filling states of ER Ca^{2+} stores are comparable. Likewise, the depletion of total intracellular Ca^{2+} stores in 0 Ca^{2+} HBSS using the Ca^{2+} ionophore ionomycin showed no difference between WT and *Stc2*$^{-/-}$ MEFs (see Fig. S4A and B). However, $[Ca^{2+}]_i$ peaks upon Ca^{2+} add back were significantly increased in *Stc2*$^{-/-}$ MEFs after store depletion with Tg or ionomycin (Fig. 2F; also see Fig. S4C). Thus, the increased intracellular Ca^{2+} levels observed in *Stc2*$^{-/-}$ MEFs after store depletion are dependent upon extracellular Ca^{2+} and are not due to differences in ER Ca^{2+} content.

To establish that the augmentation of $[Ca^{2+}]_i$ in *Stc2*$^{-/-}$ MEFs is due to increased Ca^{2+} influx rather than decreased plasma membrane Ca^{2+} pump activity, we measured Fura-2 fluorescence quenching by SOC-permeable Mn^{2+}, which permeates SOCs but is not pumped by plasma membrane Ca^{2+} ATPases (35). After establishing the rate of Mn^{2+} leak in HBSS plus Mn^{2+} (2 mM $MnCl_2$) medium, cells were challenged with Tg and the decline of Fura-2 fluorescence was monitored over time (Fig. 3A). Fura-2 quench rates were corrected for Mn^{2+} leak (Fig. 3A, inset) to obtain Tg-stimulated cation influx rates. *Stc2*$^{-/-}$ MEFs exhibited a significant increase in Mn^{2+} influx rate following store depletion, which is consistent with enhanced cation entry through SOCs (Fig. 3B).

To verify the predominant route of Ca^{2+} influx affected by the loss of *Stc2* expression, we monitored $[Ca^{2+}]_i$ in the presence of 2-aminoethyldiphenyl borate (2-APB), which inhibits Ca^{2+} entry through SOCs at concentrations of >30 μM (12). WT and *Stc2*$^{-/-}$ MEFs were challenged with Tg in the presence of extracellular Ca^{2+}, as described in the legend to Fig. 2A, with the addition of 50 μM 2-APB. The addition of 2-APB completely prevented the accumulation of $[Ca^{2+}]_i$ upon Ca^{2+} add back (Fig. 3C). Furthermore, the presence of 2-APB modified the initial biphasic response (observed immediately after Tg addition), comprising both store emptying and SOCE (Fig. 2A), to a single peak that solely represented the store depletion component (Fig. 3C). It also abrogated the elevated intracellular Ca^{2+} levels induced by Tg in the presence of external Ca^{2+} in *Stc2*$^{-/-}$ MEFs (compare Tg peaks in Fig. 2B and 3D). As a control, we also performed store depletion in 0 Ca^{2+} HBSS in the presence or absence of 2-APB and found that 2-APB does not affect store depletion by Tg (see Fig. S4D in the supplemental material). Taken together, these experiments suggest that the alteration in Ca^{2+} homeostasis observed in *Stc2*$^{-/-}$ MEFs is due to a specific increase in Ca^{2+} entry through plasma membrane SOCs.

Knockdown of *Stc2* expression potentiates SOCE in H19-7 cells. To confirm that the effect of *Stc2* expression on Ca^{2+} homeostasis is not limited to MEFs, we examined Ca^{2+} handling in rat hippocampal H19-7 cells. These cells proliferate when cultured at 33°C but differentiate upon a switch to 39°C and neuronal culture medium, and once differentiated they exhibit robust SOCE (61). We stably transduced H19-7 cells with retrovirus expressing *Stc2* short hairpin RNA (shRNA) or luciferase control shRNA and confirmed the knockdown of STC2 expression in the pooled stable cells by Western blot analysis of cell lysates and conditioned media (Fig. 4A). Following 3 days of differentiation, cells were loaded with Fura-2 and SOCE was assessed by store depletion followed by Ca^{2+} add back (Fig. 4B). Similarly to *Stc2*$^{-/-}$ MEFs, H19-7 cells with reduced STC2 expression accumulated significantly more $[Ca^{2+}]_i$ than control cells both at peak Ca^{2+} levels and at the plateau phase (Fig. 4C and D). Moreover, by monitoring Ba^{2+} influx rates, we confirmed that this difference in $[Ca^{2+}]_i$ is attributable to an increase in cation influx (Fig. 4E and F).

Overexpression of STC2 reduces SOCE. Since STC2 expression is induced by cellular stress, we generated pools of MEFs stably expressing STC2 to investigate the effect of STC2 overexpression on SOCE. As WT STC2 is readily secreted (24), we also generated stable pools of MEFs that overexpress STC2 harboring the KDEL ER retention motif ($STC2_{KDEL}$) (38) to determine if STC2 function is cell intrinsic. The overexpression of STC2 and ER retention of $STC2_{KDEL}$ was verified by the Western blot analysis of cell lysates and conditioned media (Fig. 5A) as well as by immunofluorescence staining with organelle markers (see Fig. S5 in the supplemental material). We next loaded these cells with Fura-2 and compared Ca^{2+} handling as described for Fig. 2D. Although ER Ca^{2+} stores were not different between the cell lines, we observed a significant reduction in SOCE in cells overexpressing either STC2 or $STC2_{KDEL}$ (Fig. 5B and C). Since the overexpression of ER-retained $STC2_{KDEL}$ was at least as effective as WT STC2 in reducing SOCE, these results suggest that STC2 functions intracellularly to regulate SOCE. To further confirm this notion, we examined the effect of secreted STC2 on Ca^{2+} homeostasis.

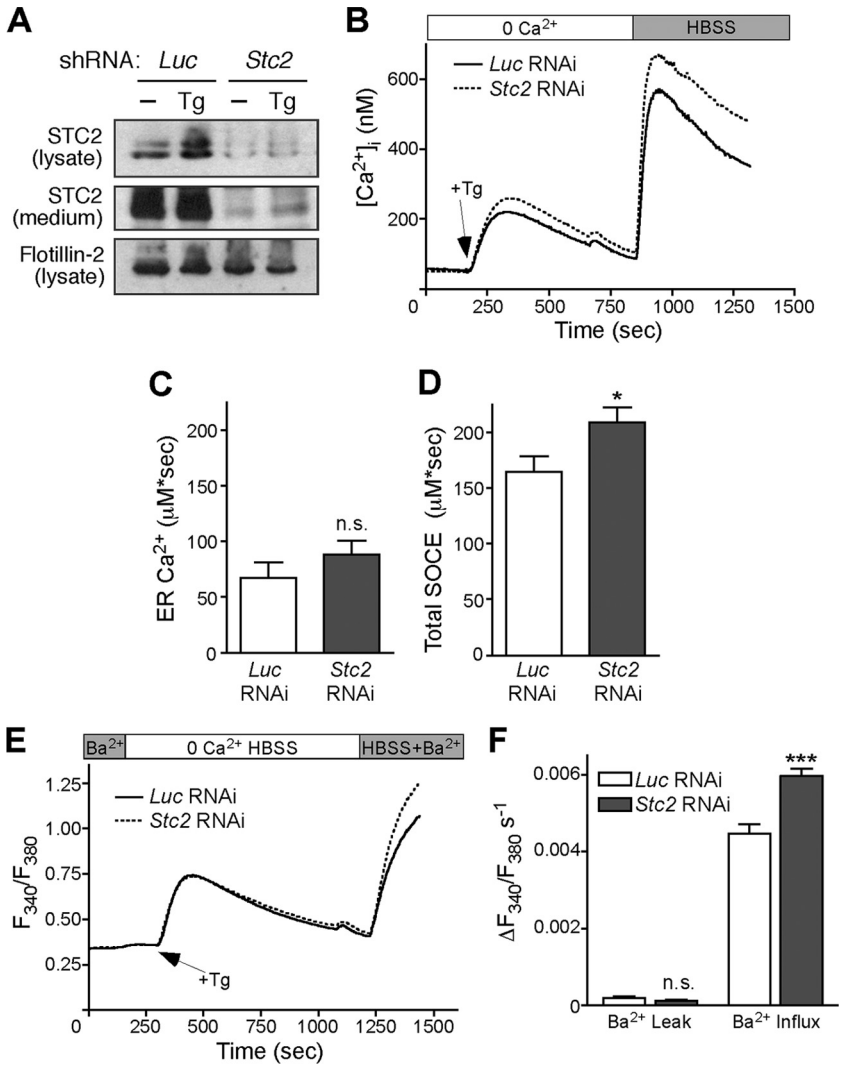

FIG. 4. Knockdown of *Stc2* expression in H19-7 cells increases SOCE. (A) Analysis of STC2 expression in stable luciferase (Luc) and STC2 RNAi pools at steady state and following treatment with Tg (300 nM) to induce ER stress. Aliquots of cell lysates and immunoprecipitates of conditioned medium were analyzed by immunoblotting. (B) Differentiated H19-7 pools of cells stably expressing STC2 or Luc shRNA were loaded with 5 μM Fura-2 AM. Cells then were perfused with 0 Ca^{2+} HBSS followed by treatment with Tg in 0 Ca^{2+} HBSS. After store depletion, HBSS was added to trigger SOCE. Each trace represents the averages from 12 experiments. Graphs represent total $[Ca^{2+}]_i$ increases (area under the curve) after Tg addition (C) or Ca^{2+} add back (D). *, $P < 0.05$ by Student's *t* test; n.s., not significant. (E) Differentiated H19-7 cells stably expressing STC2 or Luc shRNA were loaded with 5 μM Fura-2 AM. Cells then were perfused with 0 Ca^{2+} HBSS plus 2 mM $BaCl_2$ followed by treatment with Tg (1 μM) in 0 Ca^{2+} HBSS. Following store depletion, 0 Ca^{2+} HBSS plus 2 mM $BaCl_2$ was added back to trigger SOCE. Each trace represents the averages from six experiments. (F) Ba^{2+} influx rates were calculated by subtracting the linear portion of the slope before Tg addition (Ba^{2+} leak) from the slope after Tg addition. **, $P < 0.01$; ***, $P < 0.001$ (each by one-way ANOVA).

We generated pools of $Stc2^{-/-}$ MEFs stably overexpressing STC2 and collected conditioned medium from them (KO+STC2 medium) or from control $Stc2^{-/-}$ MEFs (KO medium) (Fig. 5D). We then pretreated Fura-2-loaded WT and $Stc2^{-/-}$ MEFs with KO or KO+STC2 medium before the depletion of $[Ca^{2+}]_i$ stores by Tg and monitored changes in $[Ca^{2+}]_i$ over time (Fig. 5E). While $Stc2^{-/-}$ MEFs accumulated more intracellular Ca^{2+} than WT MEFs, the presence of STC2 in the conditioned medium did not significantly affect $[Ca^{2+}]_i$ in WT or $Stc2^{-/-}$ MEFs (Fig. 5F). Taken together, these results suggest that the overexpression of STC2 reduces SOCE, likely through the modulation of an intracellular target.

STC2 interacts with STIM1. The essential components of the SOCE pathway include the ER Ca^{2+} sensor STIM1 and plasma membrane SOCs (44). Since ER-localized $STC2_{KDEL}$ was effective at reducing SOCE while secreted STC2 seemed to have no discernible effect, we hypothesized that STC2 affects SOCE through interaction with STIM1. The quantitative analysis of immunofluorescently labeled COS cells cotransfected with epitope-tagged STIM1 (YFP-STIM1) and STC2 ($STC2_{CT11}$) revealed that STC2 and STIM1 strongly colocalize within cells (Pearson's coefficient, 0.699 ± 0.041; $n = 11$) (Fig. 6A), indicating that both proteins are present within the same subcellular compartments. To test for a direct interaction be-

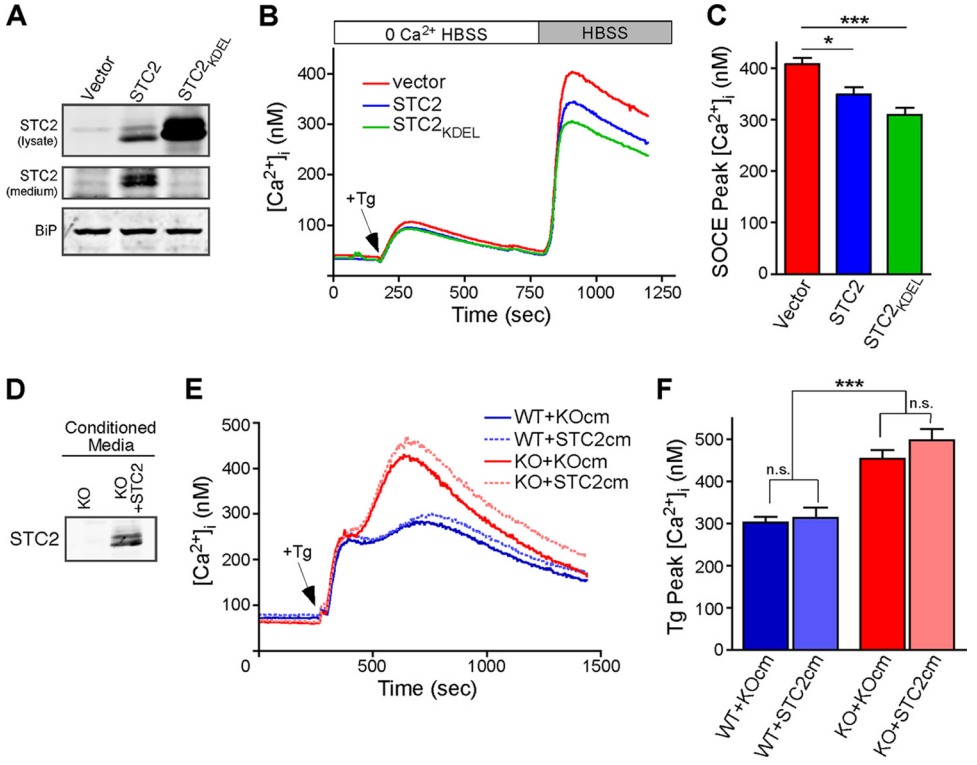

FIG. 5. Overexpression of STC2 reduces SOCE. (A) Western blot analysis of STC2 or $STC2_{KDEL}$ expression in the lysates and conditioned medium of pooled stably transduced MEFs. (B) Control and STC2-overexpressing MEFs loaded with Fura-2 were perfused in 0 Ca^{2+} HBSS before the addition of Tg (300 nM) and Ca^{2+} add back. Traces represent averages from eight experiments. (C) Quantification of $[Ca^{2+}]_i$ peaks after Ca^{2+} add back (means ± SEM). (D) Western blot analysis of conditioned medium samples from *Stc2*$^{-/-}$ MEFs (KO medium) or *Stc2*$^{-/-}$ MEFs overexpressing STC2 (KO+STC2 medium). (E) Fura-2-loaded WT or *Stc2*$^{-/-}$ MEFs were incubated in KO or KO+STC2 medium for ~10 min before Tg was added directly to the media, and $[Ca^{2+}]_i$ was monitored over time. Traces represent averages from at least 10 experiments. (F) Quantification of $[Ca^{2+}]_i$ peaks after the addition of Tg (means ± SEM). *, $P < 0.05$; **, $P < 0.01$; ***, $P < 0.001$ (each by one-way ANOVA).

tween STC2 and STIM1, we cotransfected COS cells and immunoprecipitated STIM1 using a C-terminal anti-STIM1 antibody. Western blot analysis revealed that STC2 coimmunoprecipitated with STIM1, but not when the control preimmune serum was used (Fig. 6B). Similarly, we were able to coimmunoprecipitate STIM1 with an antibody against the epitope tag on STC2 (Fig. 6C). We confirmed these results using myc-tagged STIM1 to rule out nonspecific interactions with STC2 due to the presence of the relatively large YFP epitope tag (see Fig. S6B in the supplemental material). Finally, we were unable to coimmunoprecipitate STC2 with STIM1 when lysates from cells individually transfected with STIM1 or STC2 were mixed, indicating that the binding of STC2 and STIM1 occurs within the cells and not after cell lysis (see Fig. S6A). Interestingly, we noticed that the addition of a low concentration of SDS (0.25%) produced a consistent increase in the coimmunoprecipitation of STC2 and STIM1 (Fig. 6B and C; also see Fig. S6B). While the reason for this observation is not apparent at present, we plan to explore this in future studies.

STIM1 directly senses ER Ca^{2+} levels through an N-terminal Ca^{2+} binding EF-hand domain. Upon the dissociation of Ca^{2+}, this domain undergoes significant conformational change, partially unfolding to a much less compact α-helical state that promotes oligomerization (49). Therefore, we tested the sensitivity of the coimmunoprecipitation between STC2 and STIM1 to changes in Ca^{2+} concentrations. Specifically, we performed the immunoprecipitation of STIM1 from cotransfected COS cells in the absence (EDTA) or presence of 100 nM, 1 μM, or 1 mM $CaCl_2$. We found that STC2 coimmunoprecipitated with STIM1 to a similar extent under all conditions tested, demonstrating that STC2 interaction with STIM1 is insensitive to Ca^{2+} (Fig. 6D). Consistent with this result, we also found that STC2 coimmunoprecipitated with STIM1 after Tg-induced store depletion (Fig. 6E). These results suggest that STIM1 activation and oligomerization does not preclude interaction with STC2. Therefore, we tested for coimmunoprecipitation between STC2 and the constitutively active EF-hand mutant $STIM1_{D76A}$, which oligomerizes even in the presence of replete ER stores (50, 64). We found that STC2 coimmunoprecipitated equally well with both the WT and EF-hand mutant STIM1 (Fig. 6E).

To confirm the interaction between STC2 and endogenous STIM1, we retrovirally transduced WT or *Stim1*$^{-/-}$ *Stim2*$^{-/-}$ dKO MEFs with STC2 and performed coimmunoprecipitation experiments. Under basal conditions, the coimmunoprecipitation of STC2 with endogenous STIM1 was below the limit of detection. However, we found that the induction of ER stress by the overnight treatment of cells with Tm or Tg led to a strong increase in the amount of STC2 coimmunoprecipitating with endogenous STIM1 (Fig. 6F). Similar results were obtained with treatment times as short as 4 h.

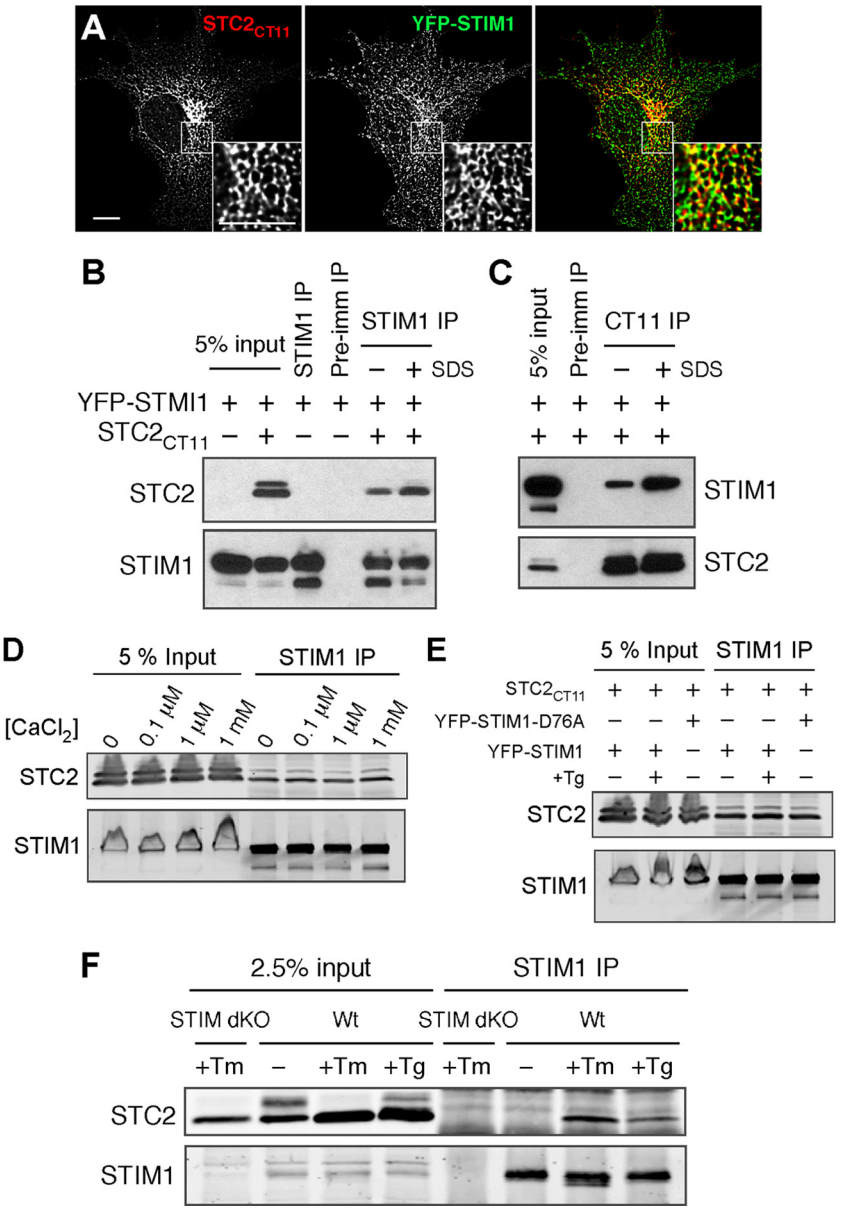

FIG. 6. STC2 interacts with STIM1. (A) Immunofluorescence labeling of COS cells coexpressing $STC2_{CT11}$ and YFP-STIM1. The maximum-intensity projection of two planes of the deconvolved Z stack is depicted. The inset shows an enlarged area indicated by a box. Scale bar, 10 μm. (B and C) COS cells were transfected as indicated and analyzed by coimmunoprecipitation using STIM1, CT11, or preimmune serum. (D) Coimmunoprecipitation of COS cells cotransfected with $STC2_{CT11}$ and YFP-STIM1 with anti-STIM1 in the presence of EDTA or 0.1 μM, 1 μM, or 1 mM $CaCl_2$. (E) Coimmunoprecipitation of COS cells cotransfected with $STC2_{CT11}$ and YFP-STIM1 or YFP-$STIM1_{D76A}$ before or after a 10-min treatment with Tg (1 μM) in 0 Ca^{2+} HBSS to deplete ER Ca^{2+} stores. (F) Coimmunoprecipitation analysis of WT or *Stim1*$^{-/-}$ *Stim2*$^{-/-}$ (Stim dKO) MEFs stably expressing $STC2_{CT11}$ under basal conditions or after overnight treatment with Tm or Tg to induce ER stress.

STC2 expression does not alter SOCE through modulation of STIM1 translocation. Upon the depletion of ER Ca^{2+} stores, STIM1 translocates in close opposition to the plasma membrane to activate SOCs. To test whether the lack of STC2 expression affects STIM1 translocation, we generated pools of WT and *Stc2*$^{-/-}$ MEFs stably expressing YFP-STIM1 and used TIRF microscopy to specifically visualize and quantify the fluorescence intensity of STIM1 located near the plasma membrane during store depletion (Fig. 7A and B). However, we found that the time to reach half-maximal translocation was indistinguishable between WT and *Stc2*$^{-/-}$ MEFs (Fig. 7C), although we observed a slightly lower rate of STIM1 translocation in *Stc2*$^{-/-}$ MEFs (Fig. 7D). The quantification of the absolute levels of translocated STIM1 showed no change under baseline conditions and a slight decrease in maximum translocated YFP-STIM1 in *Stc2*$^{-/-}$ MEFs following store depletion (Fig. 7E). Further quantification revealed that puncta size, shape, and density were similar between WT and *Stc2*$^{-/-}$ MEFs as well (Fig. 7F to H). Therefore, although STC2 physically interacts with STIM1, the loss of

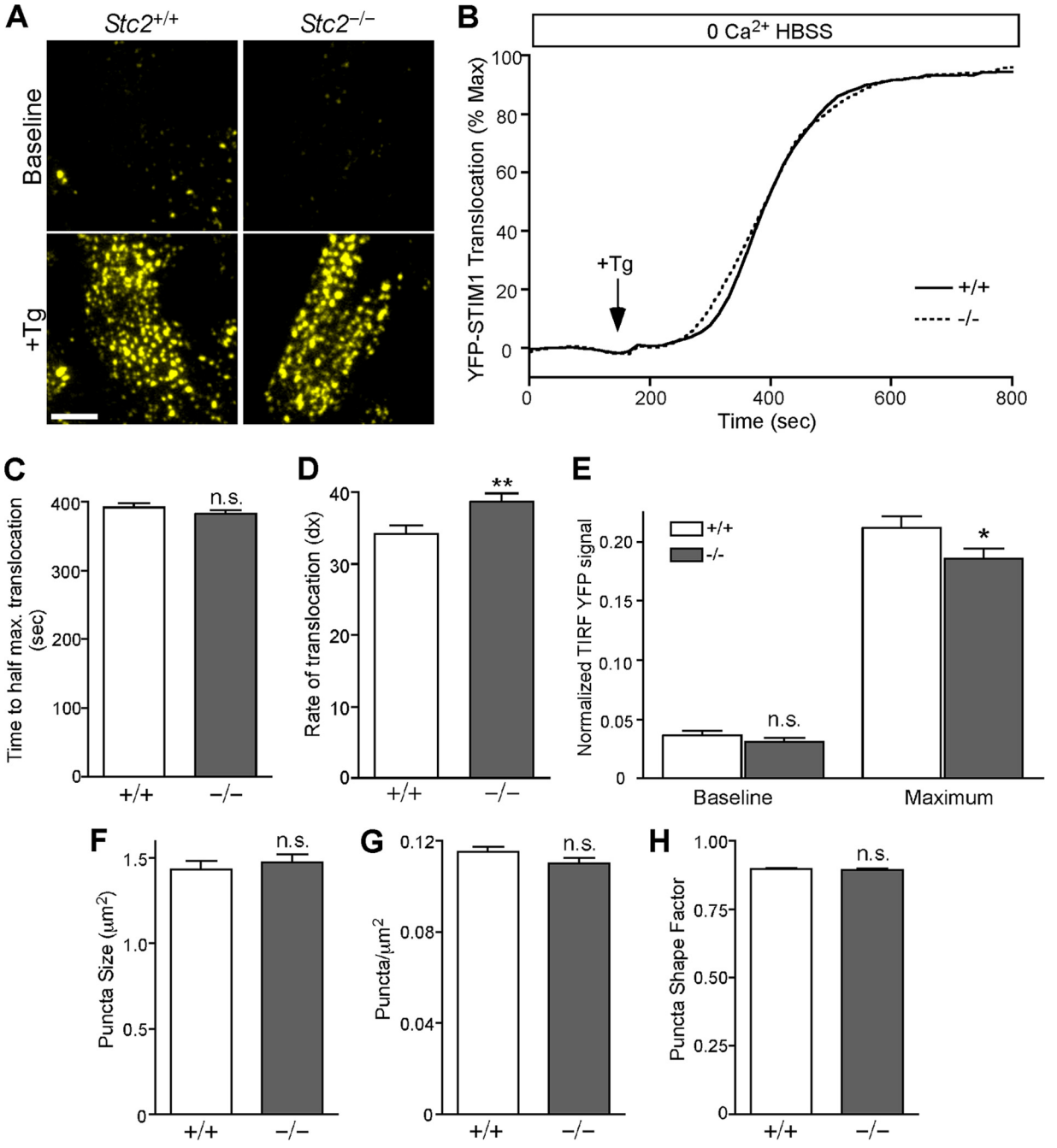

FIG. 7. STIM1 translocation is not potentiated in $Stc2^{-/-}$ MEFs following store depletion. (A) WT and $Stc2^{-/-}$ MEFs stably expressing YFP-STIM1 were imaged by TIRF microscopy. Representative TIRF images are shown before and after ER Ca^{2+} store depletion by the addition of Tg. Scale bar, 10 μm. (B) Time-lapse TIRF images of transfected WT and $Stc2^{-/-}$ MEFs treated with Tg (300 nM) in 0 Ca^{2+} HBSS were acquired to measure the translocation of YFP-STIM1 to puncta near the plasma membrane. Total YFP TIRF intensity was quantified, and STIM1 translocation was plotted over time and normalized to the maximum YFP-STIM1 TIRF signal. Traces represent the averages from 12 experiments, with ~6 to 12 cells/experiment. (C and D) Data from individual cells were fit using a Boltzmann sigmoidal function, and the time to half-maximal translocation (C) and the rate constant (*dX*) (where *dX* is equal to the change in time corresponding to the greatest change in STIM1 translocation, such that larger *dX* values correspond to lower rates of translocation) (D) were calculated and compared between WT and $Stc2^{-/-}$ MEFs. (E) Total translocated STIM1 values at baseline and at maximum were quantified by the normalization of TIRF YFP signals to wide-field fluorescence. n.s., not significant. *, $P < 0.05$; **, $P < 0.01$ (each by Student's *t* test). (F to H) Quantification of YFP-STIM1 puncta size (F), density (G), and shape factor (H), where 1 is equal to a perfect circle, in WT and $Stc2^{-/-}$ MEFs following store depletion.

STC2 does not increase SOCE by the potentiation of STIM1 translocation.

The overexpression of STIM1 has been shown to produce modest increases in SOCE in HEK, HeLa, and Jurkat cells (32, 42, 46, 47). To determine if STC2 increases SOCE by affecting STIM1 expression, we analyzed levels of endogenous STIM1 in WT and $Stc2^{-/-}$ MEFs. Contrary to our expectation, we found that STIM1 expression was reduced by ~40% in $Stc2^{-/-}$

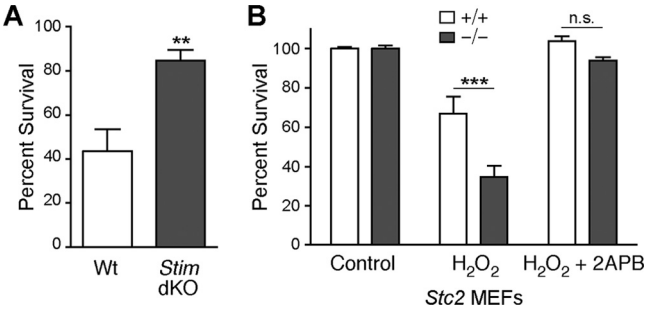

FIG. 8. Susceptibility of *Stc2*$^{-/-}$ MEFs to oxidative stress is rescued by inhibition of SOCE. (A) WT and *Stim1*$^{-/-}$ *Stim2*$^{-/-}$ (*Stim* dKO) MEFs were treated with H_2O_2 (200 μM) for 16 h, and cell survival was quantified relative to that of untreated controls using a colorimetric WST-8 assay. **, $P < 0.01$ by Student's *t* test. (B) Cell survival of WT and *Stc2*$^{-/-}$ MEFs was quantified following treatment with H_2O_2 (200 μM) for 16 h in the presence or absence of 100 μM 2-APB. Data represent the means ± SEM from three experiments, each performed in triplicate. ***, $P < 0.001$ by one-way ANOVA; n.s., not significant.

MEFs compared to that of the WT (see Fig. S7 in the supplemental material). Thus, the loss of STC2 does not increase SOCE through increased expression of STIM1. Rather, this result suggests that the negative tone on SOCE provided by STC2 is underestimated in our experiments, as SOCE was increased in *Stc2*$^{-/-}$ MEFs despite reduced STIM1 levels.

Blockade of SOCE rescues *Stc2*$^{-/-}$ MEF susceptibility to oxidative stress. Alterations in cellular Ca^{2+} homeostasis, especially those that lead to increases in cytoplasmic Ca^{2+} levels, underlie diverse injury and disease states (14). Importantly, STIM1 recently was demonstrated to be a target of S-glutathionylation during oxidative stress, and this modification leads to the constitutive activation of SOCE and increased cell death (20). Likewise, we found that *Stim1*$^{-/-}$ *Stim2*$^{-/-}$ MEFs are protected from oxidative stress-induced cell death (Fig. 8A). Since our results indicate that STC2 functions as a negative modulator of SOCE, we hypothesized that increased Ca^{2+} influx due to the loss of STC2 expression is responsible for the enhanced susceptibility of *Stc2*$^{-/-}$ MEFs to oxidative stress. To test this possibility, we measured the susceptibility of WT and *Stc2*$^{-/-}$ MEFs to oxidative stress in the presence of the SOCE inhibitor 2-APB. The induction of cell death elicited by H_2O_2 was blocked by the coincubation of WT MEFs with 100 μM 2-APB (Fig. 8B). More importantly, incubation with 2-APB also was able to block cell death in *Stc2*$^{-/-}$ MEFs. These results indicate that Ca^{2+} influx through SOCE is an essential component of cell death triggered by oxidative stress, and that the enhanced susceptibility of *Stc2*$^{-/-}$ MEFs to H_2O_2 very likely is attributable to the observed increase in SOCE.

DISCUSSION

In this study, we provide the first evidence for a direct role for STC2 in the regulation of cellular Ca^{2+} homeostasis. Previously we reported that the expression of STC2 is upregulated in mammalian cells by ER stress, oxidative stress, and hypoxia, and that STC2 is a critical survival component of the UPR (23). However, the precise cellular and molecular function for STC2 has remained elusive. Here, we report that fibroblasts derived from *Stc2*$^{-/-}$ mice accumulate increased intracellular Ca^{2+} following store depletion. Our data demonstrate that this increase in $[Ca^{2+}]_i$ levels results from an increase in Ca^{2+} influx and is not due to alterations in intracellular Ca^{2+} stores. Furthermore, we have found that the increased Ca^{2+} influx occurs specifically through SOCs, as it can be completely blocked by the SOCE inhibitor 2-APB. Increased SOCE also was observed in the rat hippocampal H19-7 cell line with the knockdown of *Stc2* expression. Conversely, the overexpression of STC2 in MEFs resulted in a reduction of SOCE. Taken together, these experiments suggest that STC2 functions as a negative regulator of Ca^{2+} influx through SOCs.

It has been documented that Stanniocalcin functions as an endocrine regulator of gill Ca^{2+} uptake in fish (55). While a few studies have proposed similar functions for mammalian STCs (33, 40), no abnormalities in serum Ca^{2+} or phosphate levels were observed in *Stc1*$^{-/-}$, *Stc2*$^{-/-}$, or *Stc1*$^{-/-}$ *Stc2*$^{-/-}$ mice as well as transgenic mice overexpressing STC2 (8, 9, 17). Thus, results from these *Stc2* mouse models indicated a lack of conservation of endocrine function for STC2 in mineral homeostasis in mammals. However, our Ca^{2+} imaging assays demonstrate that mammalian STC2 regulates Ca^{2+} homeostasis by the modulation of SOCE at the cellular level. Although mammalian STC2 is a secreted protein, we found that $STC2_{KDEL}$, which is retained in the ER and does not get secreted, was as effective as wild-type STC2 in reducing SOCE, suggesting an intracellular target of STC2 action.

Consistently with the notion of cell-intrinsic STC2 function, we found substantial overlap in the intracellular localization as well as an interaction between STC2 and STIM1, an essential component of the SOCE pathway (32, 46). STIM1 serves as both the sensor of ER Ca^{2+} levels and the activator of plasma membrane SOCs (6). Recent work has identified several SOCE regulatory proteins that appear to function by binding STIM1 (19, 48, 59, 60). However, to our knowledge, STC2 represents the first ER luminal protein with the ability to both bind STIM1 and regulate the overall magnitude of SOCE. Although STIM1 and STIM2 interact with and gate SOCs through domains within the C terminus that are oriented toward the cytosol, domain-swapping studies reveal that a short stretch of flexible random coil domains at the extreme N terminus of STIM proteins (oriented toward the lumen) confer dramatically different Orai1 activation kinetics. Notably, the physiological control of the overall magnitude of SOCE exerted by STIM1 and STIM2 mediated by the N-terminal flexible random coil domain occurred independently of changes in ER Ca^{2+}, STIM clustering, or interaction with Orai1 (65). Since we did not find any potentiation of STIM1 translocation in *Stc2*$^{-/-}$ MEFs, we hypothesize that the binding of STC2 to STIM1 within the ER lumen modifies the intrinsic function of the extreme N terminus of STIM1, leading to changes in the overall magnitude of SOCE after store depletion. This is consistent with our observation that STIM1 coimmunoprecipitates with the core glycosylated immature form of STC2 (Fig. 6B and D) as well as ER-retained $STC2_{KDEL}$ (data not shown). Furthermore, under the conditions employed in our experiments, STC2 does not coimmunoprecipitate Orai1.

Our attempts to map the interacting domains in STC2 and

luminal domain of STIM1 using deletion mutants have not been successful because of the intramolecular associations within these proteins. The luminal domain of STIM1 has a complex molecular structure, where the EF and SAM domains fold cooperatively. Although it is possible to express recombinant proteins that correspond to the EF1-SAM domain of STIM1 (residues Ser58 to Gly201), the expression of the isolated canonical Ca^{2+} binding EF-hand 1, hidden EF2, or SAM domain results in unfolded protein or highly labile protein (49, 50). Structural analysis reveals that this instability is consistent with EF-hand-SAM intramolecular association and the mutually linked folding and stability of the region encompassing EF1-SAM domains (50). Similarly, the expression of experimental deletion mutants of STC2 is problematic due to the presence of multiple intra- and intermolecular disulfide bridges in STC2 (21). However, our coimmunoprecipitation experiments do provide some insights. STC2 was found to coimmunoprecipitate with STIM1 across a range of Ca^{2+} concentrations. Furthermore, STC2 also could be coimmunoprecipitated with STIM1 following store depletion with Tg or with the constitutively active EF-hand mutant $STIM1_{D76A}$. Taken together, these experiments suggest that STC2 is capable of binding STIM1 in both resting and activated conformations and thus is situated to directly regulate STIM1 function during SOCE.

We also found that the binding of endogenous STIM1 with STC2 is increased by ER stress-inducing agents. This increase was seen with as little as 4 h of treatment with Tm or Tg and persisted with overnight treatment. It is possible that this increase in binding is attributable to an elevation in cell-associated STC2 resulting from the impaired secretion of this protein (as is the case with many other proteins) during ER stress (see Fig. S6C and D in the supplemental material). However, the increase in coimmunoprecipitated STC2 induced by treatment appears to be significantly greater than the increase in STC2 observed in the input lysate. Alternatively, both Tg and Tm perturb the luminal protein folding environment, and this could favor alternative conformations of STC2 or STIM1 that lead to increased association. Such a mechanism for regulated association and dissociation has been demonstrated previously for the binding of the ER luminal chaperone BiP to the transmembrane signal transduction kinases PERK and IRE1 during the UPR (2). The N terminus of STIM1 undergoes significant conformational change associated with Ca^{2+} binding (or unbinding) (49, 50). Since STC2 and STIM1 can be coimmunoprecipitated across a range of concentrations of Ca^{2+}, it seems unlikely that Ca^{2+}-induced conformational changes in STIM1 that occur during store depletion, with the short-term application of Tg (10 min), mediate the increased association of STC2 (Fig. 6E). Therefore, we favor the hypothesis that changes in STC2 folding mediated by ER stress, such as following prolonged incubations with Tg or Tm (Fig. 6F), promote its interaction with STIM1.

We and others have shown previously that the expression of STC2 is induced during cellular stress, and this induction has a cytoprotective function (23, 28, 30). The data presented here are consistent with the idea that STC2 limits the STIM1-mediated activation of Ca^{2+} influx during periods of cellular stress, thus promoting cellular survival. An increase in STC2 binding to STIM1 in cells treated with Tg or Tm, two agents that cause ER stress, supports this notion. In addition to STC2, recent work has identified a potential role for STIM1 in the cellular stress response. Specifically, STIM1 is a target of S-glutathionylation during oxidative stress, and this modification leads to the store-independent translocation of STIM1, activation of SOCs, and increased cellular vulnerability to stress (20). In agreement with this data, we were able to confirm that $Stim1^{-/-}$ $Stim2^{-/-}$ MEFs are protected from H_2O_2-induced cell death. Since $Stc2^{-/-}$ MEFs lack the negative regulation of STIM1-mediated Ca^{2+} influx and show increased susceptibility to oxidative stress-induced cell death, we hypothesized that this function of STC2 underlies its cytoprotective properties. Therefore, we tested the susceptibility of $Stc2^{-/-}$ MEFs to H_2O_2-induced cell death in the presence of the SOCE inhibitor 2-APB and found that the blockade of Ca^{2+} influx fully rescued the susceptibility of these cells. Therefore, STC2-mediated negative regulation of SOCE is likely to be important for cell viability during periods of oxidative stress. It is known that a complex set of transcriptional and posttranscriptional events, collectively referred to as the integrated stress response, coordinate cell survival following ER and oxidative stress (25, 45). Previously we uncovered the upregulation of STC2 following ER and oxidative stress and reported that STC2 upregulation offered cytoprotection from stress-induced apoptotic cell death (23). The results outlined here demonstrate that the mechanism by which STC2 exerts its cytoprotective property under conditions of cellular stress is through the negative modulation of SOCE.

In addition to a role in the cellular stress response, STC2 expression has been correlated with the development or severity of several types of cancer, including breast, prostate, renal, colorectal, and ovarian carcinomas (4, 5, 22, 36, 51). In fact, several of these studies have proposed using STC2 expression as a prognostic marker (5, 15, 26, 36). Although there is a clear correlation between STC2 levels and cancer progression, most of these studies have not addressed the functional significance of elevated STC2 expression. Some reports using cancer cell lines, however, have proposed that STC2 promotes the invasiveness and metastasis of cancer cells, although the exact mechanism for this effect is not clear (26, 29, 53). Our current study has identified SOCE as an important molecular pathway regulated by STC2, with STIM1 as a direct binding partner. Interestingly, the short interfering RNA (siRNA) downregulation of STIM1 has been shown to decrease cancer cell migration *in vitro* and inhibit tumor metastasis *in vivo* (63), raising the question of how a positive regulator (STIM1) and a negative regulator (STC2) of SOCE both can promote cancer progression. The answer may lie in the dual nature of Ca^{2+} as a signal transducer, whereby moderate elevations of Ca^{2+} promote cell proliferation, migration, and invasion and higher Ca^{2+} elevations promote apoptosis. One of the central requirements for the successful progression of tumor cells is the development of methods to escape apoptosis. A high level of STC2 expression would protect tumor cells by ensuring that SOCE is not elevated to the point that it would induce Ca^{2+}-dependent apoptosis. A similar process occurs for the stress-induced p53 proteins, where cell stress induces

moderate levels of p53, leading to the transcription of numerous genes that help the cell deal with the stress. However, because too-high levels of p53 can induce apoptosis, an inhibitor of p53 (mdm-2) is produced in parallel to act as a buffer to prevent p53 from inducing apoptosis under inappropriate conditions (54). Therefore, the negative regulation of SOCE by STC2 may represent an important mechanism by which STC2 expression can help tumor cells evade apoptosis and aide in cancer progression.

ACKNOWLEDGMENTS

We thank Tobias Meyer (Stanford University) for the gift of YFP-STIM1 plasmid. We thank Peter Pytel (University of Chicago) for the pathological examination of tissue and Breanne Kassarjian for the maintenance of the mouse colony.

This work was supported by National Institutes of Health grants NS053853 and AG021495 (to G.T.). W.Z. is the recipient of NRSA award NS065660.

REFERENCES

1. **Berridge, M. J., M. D. Bootman, and H. L. Roderick.** 2003. Calcium signalling: dynamics, homeostasis and remodelling. Nat. Rev. Mol. Cell Biol. **4:**517–529.
2. **Bertolotti, A., Y. Zhang, L. M. Hendershot, H. P. Harding, and D. Ron.** 2000. Dynamic interaction of BiP and ER stress transducers in the unfolded-protein response. Nat. Cell Biol. **2:**326–332.
3. **Bolte, S., and F. P. Cordelieres.** 2006. A guided tour into subcellular colocalization analysis in light microscopy. J. Microsc. **224:**213–232.
4. **Bouras, T., et al.** 2002. Stanniocalcin 2 is an estrogen-responsive gene coexpressed with the estrogen receptor in human breast cancer. Cancer Res. **62:**1289–1295.
5. **Buckanovich, R. J., et al.** 2007. Tumor vascular proteins as biomarkers in ovarian cancer. J. Clin. Oncol. **25:**852–861.
6. **Cahalan, M. D.** 2009. STIMulating store-operated Ca(2+) entry. Nat. Cell Biol. **11:**669–677.
7. **Carafoli, E., and M. Brini (ed.).** 2007. Calcium signalling and disease. Subcellular biochemistry, vol. 45. Springer, New York, NY.
8. **Chang, A. C., J. Cha, F. Koentgen, and R. R. Reddel.** 2005. The murine stanniocalcin 1 gene is not essential for growth and development. Mol. Cell. Biol. **25:**10604–10610.
9. **Chang, A. C., et al.** 2008. The murine stanniocalcin 2 gene is a negative regulator of postnatal growth. Endocrinology **149:**2403–2410.
10. **Cheng, K. T., X. Liu, H. L. Ong, and I. S. Ambudkar.** 2008. Functional requirement for Orai1 in store-operated TRPC1-STIM1 channels. J. Biol. Chem. **283:**12935–12940.
11. **Clapham, D. E.** 2007. Calcium signaling. Cell **131:**1047–1058.
12. **DeHaven, W. I., J. T. Smyth, R. R. Boyles, G. S. Bird, and J. W. Putney, Jr.** 2008. Complex actions of 2-aminoethyldiphenyl borate on store-operated calcium entry. J. Biol. Chem. **283:**19265–19273.
13. **De Niu, P., et al.** 2000. Development of a human stanniocalcin radioimmunoassay: serum and tissue hormone levels and pharmacokinetics in the rat. Mol. Cell Endocrinol. **162:**131–144.
14. **Dong, Z., P. Saikumar, J. M. Weinberg, and M. A. Venkatachalam.** 2006. Calcium in cell injury and death. Annu. Rev. Pathol. **1:**405–434.
15. **Esseghir, S., et al.** 2007. Identification of NTN4, TRA1, and STC2 as prognostic markers in breast cancer in a screen for signal sequence encoding proteins. Clin. Cancer Res. **13:**3164–3173.
16. **Feske, S., C. Picard, and A. Fischer.** 2010. Immunodeficiency due to mutations in ORAI1 and STIM1. Clin. Immunol. **135:**169–182.
17. **Gagliardi, A. D., E. Y. Kuo, S. Raulic, G. F. Wagner, and G. E. DiMattia.** 2005. Human stanniocalcin-2 exhibits potent growth-suppressive properties in transgenic mice independently of growth hormone and IGFs. Am. J. Physiol. Endocrinol. Metab. **288:**E92–E105.
18. **Gong, P., et al.** 2010. Mutation analysis of the presenilin 1 N-terminal domain reveals a broad spectrum of gamma-secretase activity toward amyloid precursor protein and other substrates. J. Biol. Chem. **285:**38042–38052.
19. **Grigoriev, I., et al.** 2008. STIM1 is a MT-plus-end-tracking protein involved in remodeling of the ER. Curr. Biol. **18:**177–182.
20. **Hawkins, B. J., et al.** 2010. S-glutathionylation activates STIM1 and alters mitochondrial homeostasis. J. Cell Biol. **190:**391–405.
21. **Hulova, I., and H. Kawauchi.** 1999. Assignment of disulfide linkages in chum salmon stanniocalcin. Biochem. Biophys. Res. Commun. **257:**295–299.
22. **Ieta, K., et al.** 2009. Clinicopathological significance of stanniocalcin 2 gene expression in colorectal cancer. Int. J. Cancer **125:**926–931.
23. **Ito, D., et al.** 2004. Characterization of stanniocalcin 2, a novel target of the mammalian unfolded protein response with cytoprotective properties. Mol. Cell Biol. **24:**9456–9469.
24. **Jellinek, D. A., et al.** 2000. Stanniocalcin 1 and 2 are secreted as phosphoproteins from human fibrosarcoma cells. Biochem. J. **350:**453–461.
25. **Kaufman, R. J., S. H. Back, B. Song, J. Han, and J. Hassler.** 2010. The unfolded protein response is required to maintain the integrity of the endoplasmic reticulum, prevent oxidative stress and preserve differentiation in beta-cells. Diabetes Obes. Metab. **12**(Suppl. 2):99–107.
26. **Kita, Y., et al.** 2011. STC2: a predictive marker for lymph node metastasis in esophageal squamous-cell carcinoma. Ann. Surg. Oncol. **18:**261–272.
27. **Kwan, C. Y., and J. W. Putney, Jr.** 1990. Uptake and intracellular sequestration of divalent cations in resting and methacholine-stimulated mouse lacrimal acinar cells. Dissociation by Sr2+ and Ba2+ of agonist-stimulated divalent cation entry from the refilling of the agonist-sensitive intracellular pool. J. Biol. Chem. **265:**678–684.
28. **Law, A. Y., et al.** 2008. Epigenetic and HIF-1 regulation of stanniocalcin-2 expression in human cancer cells. Exp. Cell Res. **314:**1823–1830.
29. **Law, A. Y., and C. K. Wong.** 2010. Stanniocalcin-2 promotes epithelial-mesenchymal transition and invasiveness in hypoxic human ovarian cancer cells. Exp. Cell Res. **316:**3425–3434.
30. **Leonard, M. O., D. C. Cottell, C. Godson, H. R. Brady, and C. T. Taylor.** 2003. The role of HIF-1 alpha in transcriptional regulation of the proximal tubular epithelial cell response to hypoxia. J. Biol. Chem. **278:**40296–40304.
31. **Liao, Y., et al.** 2009. A role for Orai in TRPC-mediated Ca2+ entry suggests that a TRPC:Orai complex may mediate store and receptor operated Ca2+ entry. Proc. Natl. Acad. Sci. U. S. A. **106:**3202–3206.
32. **Liou, J., et al.** 2005. STIM is a Ca2+ sensor essential for Ca2+-store-depletion-triggered Ca2+ influx. Curr. Biol. **15:**1235–1241.
33. **Madsen, K. L., et al.** 1998. Stanniocalcin: a novel protein regulating calcium and phosphate transport across mammalian intestine. Am. J. Physiol. **274:** G96–102.
34. **Meckler, X., et al.** 2010. Reduced Alzheimer's disease ss-amyloid deposition in transgenic mice expressing S-palmitoylation-deficient APH1aL and nicastrin. J. Neurosci. **30:**16160–16169.
35. **Merritt, J. E., R. Jacob, and T. J. Hallam.** 1989. Use of manganese to discriminate between calcium influx and mobilization from internal stores in stimulated human neutrophils. J. Biol. Chem. **264:**1522–1527.
36. **Meyer, H. A., et al.** 2009. Identification of stanniocalcin 2 as prognostic marker in renal cell carcinoma. Eur. Urol. **55:**669–678.
37. **Morita, S., T. Kojima, and T. Kitamura.** 2000. Plat-E: an efficient and stable system for transient packaging of retroviruses. Gene Ther. **7:**1063–1066.
38. **Munro, S., and H. R. Pelham.** 1987. A C-terminal signal prevents secretion of luminal ER proteins. Cell **48:**899–907.
39. **Oh-hora, M., and A. Rao.** 2008. Calcium signaling in lymphocytes. Curr. Opin. Immunol. **20:**250–258.
40. **Olsen, H. S., M. A. Cepeda, Q. Q. Zhang, C. A. Rosen, and B. L. Vozzolo.** 1996. Human stanniocalcin: a possible hormonal regulator of mineral metabolism. Proc. Natl. Acad. Sci. U. S. A. **93:**1792–1796.
41. **Paschen, W.** 2001. Dependence of vital cell function on endoplasmic reticulum calcium levels: implications for the mechanisms underlying neuronal cell injury in different pathological states. Cell Calcium **29:**1–11.
42. **Peinelt, C., et al.** 2006. Amplification of CRAC current by STIM1 and CRACM1 (Orai1). Nat. Cell Biol. **8:**771–773.
43. **Prakriya, M., et al.** 2006. Orai1 is an essential pore subunit of the CRAC channel. Nature **443:**230–233.
44. **Putney, J. W., Jr.** 2007. Recent breakthroughs in the molecular mechanism of capacitative calcium entry (with thoughts on how we got here). Cell Calcium. **42:**103–110.
45. **Ron, D., and P. Walter.** 2007. Signal integration in the endoplasmic reticulum unfolded protein response. Nat. Rev. Mol. Cell Biol. **8:**519–529.
46. **Roos, J., et al.** 2005. STIM1, an essential and conserved component of store-operated Ca2+ channel function. J. Cell Biol. **169:**435–445.
47. **Soboloff, J., et al.** 2006. Orai1 and STIM reconstitute store-operated calcium channel function. J. Biol. Chem. **281:**20661–20665.
48. **Srikanth, S., et al.** 2010. A novel EF-hand protein, CRACR2A, is a cytosolic Ca2+ sensor that stabilizes CRAC channels in T cells. Nat. Cell Biol. **12:**436–446.
49. **Stathopulos, P. B., G. Y. Li, M. J. Plevin, J. B. Ames, and M. Ikura.** 2006. Stored Ca2+ depletion-induced oligomerization of stromal interaction molecule 1 (STIM1) via the EF-SAM region: an initiation mechanism for capacitive Ca2+ entry. J. Biol. Chem. **281:**35855–35862.
50. **Stathopulos, P. B., L. Zheng, G. Y. Li, M. J. Plevin, and M. Ikura.** 2008. Structural and mechanistic insights into STIM1-mediated initiation of store-operated calcium entry. Cell **135:**110–122.
51. **Tamura, K., et al.** 2009. Stanniocalcin 2 overexpression in castration-resistant prostate cancer and aggressive prostate cancer. Cancer Sci. **100:**914–919.
52. **Thastrup, O., P. J. Cullen, B. K. Drobak, M. R. Hanley, and A. P. Dawson.** 1990. Thapsigargin, a tumor promoter, discharges intracellular Ca2+ stores by specific inhibition of the endoplasmic reticulum Ca2(+)-ATPase. Proc. Natl. Acad. Sci. U. S. A. **87:**2466–2470.
53. **Volland, S., W. Kugler, L. Schweigerer, J. Wilting, and J. Becker.** 2009. Stanniocalcin 2 promotes invasion and is associated with metastatic stages in neuroblastoma. Int. J. Cancer **125:**2049–2057.

54. **Wade, M., Y. V. Wang, and G. M. Wahl.** 2010. The p53 orchestra: Mdm2 and Mdmx set the tone. Trends Cell Biol. **20:**299–309.
55. **Wagner, G. F., and G. E. Dimattia.** 2006. The stanniocalcin family of proteins. J. Exp. Zool. A Comp. Exp. Biol. **305:**769–780.
56. **Wagner, G. F., et al.** 1988. Comparative biochemistry and physiology of teleocalcin from sockeye and coho salmon. Gen. Comp. Endocrinol. **72:**237–246.
57. **Wagner, G. F., M. Hampong, C. M. Park, and D. H. Copp.** 1986. Purification, characterization, and bioassay of teleocalcin, a glycoprotein from salmon corpuscles of Stannius. Gen. Comp. Endocrinol. **63:**481–491.
58. **Wagner, G. F., C. Milliken, H. G. Friesen, and D. H. Copp.** 1991. Studies on the regulation and characterization of plasma stanniocalcin in rainbow trout. Mol. Cell Endocrinol. **79:**129–138.
59. **Walsh, C. M., M. K. Doherty, A. V. Tepikin, and R. D. Burgoyne.** 2010. Evidence for an interaction between Golli and STIM1 in store-operated calcium entry. Biochem. J. **430:**453–460.
60. **Woodward, O. M., et al.** 2010. Identification of a polycystin-1 cleavage product, P100, that regulates store operated Ca entry through interactions with STIM1. PLoS One **5:**e12305.
61. **Wu, X., T. K. Zagranichnaya, G. T. Gurda, E. M. Eves, and M. L. Villereal.** 2004. A TRPC1/TRPC3-mediated increase in store-operated calcium entry is required for differentiation of H19-7 hippocampal neuronal cells. J. Biol. Chem. **279:**43392–43402.
62. **Yahata, K., et al.** 2003. Regulation of stanniocalcin 1 and 2 expression in the kidney by klotho gene. Biochem. Biophys. Res. Commun. **310:**128–134.
63. **Yang, S., J. J. Zhang, and X. Y. Huang.** 2009. Orai1 and STIM1 are critical for breast tumor cell migration and metastasis. Cancer Cell **15:**124–134.
64. **Zhang, S. L., et al.** 2005. STIM1 is a Ca2+ sensor that activates CRAC channels and migrates from the Ca2+ store to the plasma membrane. Nature **437:**902–905.
65. **Zhou, Y., et al.** 2009. The short N-terminal domains of STIM1 and STIM2 control the activation kinetics of Orai1 channels. J. Biol. Chem. **284:**19164–19168.